



Offshore expansion of the Brazilian coastal upwelling zones during Marine Isotope Stage 5



Douglas V.O. Lessa^{a,b}, Thiago P. Santos^a, Igor M. Venancio^{a,b,c}, Ana Luiza S. Albuquerque^{a,*}

^a Programa de Pós-Graduação em Geoquímica Ambiental, Universidade Federal Fluminense, Niterói 24.020-141, Brazil

^b MARUM — Center for Marine Environmental Sciences and Faculty of Geosciences, University of Bremen, D-28359 Bremen, Germany

^c Center for Weather Forecasting and Climate Studies (CPTEC), National Institute for Space Research (INPE), Rodovia Pres. Dutra, km 39, 12.630-000 Cachoeira Paulista, SP, Brazil

ARTICLE INFO

Keywords:

Upwelling
Planktonic foraminifera
Brazil Current
Eccentricity
Paleoceanography

ABSTRACT

Paleoceanographic reconstructions in upwelling regions can provide relevant information about changes in primary productivity, ocean–atmosphere interactions and the carbon budget. Here, we assessed new data on planktonic foraminifera from a sediment core located near to coastal upwelling zones along the Brazilian coast. Our new data was combined with previous records to reveal the state of upwelling systems along the western South Atlantic margin throughout the last two deglacial and interglacial periods *sensu lato*. Despite the contemporary oligotrophic scenario of the Santos Basin, a remarkably high relative abundance of *Globigerina bulloides* and low temperatures at a depth of 100 m indicated upwelling conditions similar to current shelf upwelling zones from 130 to 90 kyr BP. Comparing these results with previous studies, we argue that Brazilian shelf upwelling zones expanded offshore between 20 and 28°S. We develop two conceptual scenarios to characterize the system: (1) during Marine Isotopic Stage (MIS 5), the system expanded along the continental margin between 20 and 28°S following the eccentricity maximum; and (2) after 20 kyr BP, the system retracted to current continental shelf zones. We propose a new mechanism whereby variation of the Earth's eccentricity, which drives seasonality, is the main factor controlling expansion or retraction of the Brazilian upwelling system. Absence of such conditions in more recent periods supports our model and indicates that current upwelling zones are the remnants of a larger upwelling system. However, more studies are required to better define the latitudinal boundaries of the Brazilian upwelling system in the past and its possible influences over the regional carbon budget.

1. Introduction

Upwelling zones encompass only 2% of the world's oceans. However, 7% of total oceanic primary production and about 20% of fishery captures occur in upwelling systems (Pauly and Christensen, 1995; Wang et al., 2015). Well-known upwelling systems are located on the eastern margins of the Pacific and Atlantic oceans, such as the Humboldt and Benguela upwelling systems, respectively (Heymans and Baird, 2000; Thiel et al., 2007; Wang et al., 2015). Western oceanic margins also host important upwelling systems, such as the Cariaco and Arabian systems (Muller-Karger et al., 2001; Peeters et al., 2002). Western border upwelling systems are usually related to the action of trade winds and/or instabilities of ocean surface fluxes (e.g. Campos et al., 2000), so they are highly sensitive to ocean–atmosphere coupling. Thus, intensification of the land–sea pressure gradient and meridional wind stress have the capacity to enhance upwelling around the world

(Bakun, 1990; Narayan et al., 2010).

Variations in wind strength have also been documented as altering upwelling intensity (e.g. Little et al., 1997a, 1997b). Where upwelling is strongly linked to regional wind systems, past changes in ocean–atmosphere interactions and variability of the regional wind system can be indirectly achieved by upwelling reconstructions. In eastern boundary upwelling systems, studies have revealed that upwelling was stronger during glacial stages due to intensification of regional trade winds (Abrantes, 1991, 1992; Weber et al., 1995; Wells and Okada, 1996; Kim et al., 2003; Romero et al., 2008; Matsuzaki et al., 2011). However, Anderson and Prell (1993) reported stronger events in the Oman upwelling system (western boundary) during interglacial stages due to increased equatorial-originating SW monsoonal winds.

One of the most powerful tools to reconstruct past upwelling variations is faunal analysis of planktonic foraminifera, since some species are tightly linked to strong upwelling events (e.g. Salgueiro et al.,

* Corresponding author at: Programa de Geoquímica Ambiental, Universidade Federal Fluminense, Outeiro São João Baptista s/n., Niterói, 24.020-141 Rio de Janeiro, Brazil.
E-mail address: ana_albuquerque@id.uff.br (A.L.S. Albuquerque).

2008). Furthermore, faunal analysis allows a straightforward estimation of ocean temperature (Kucera, 2007). The most common species that indicate changes in upwelling intensity are *Neoglobobulimina paucyderma* and *Globigerina bulloides* (Thunnell and Sautter, 1992; Little et al., 1997a; Marchant et al., 1999). In western boundary upwelling systems, *G. bulloides* alone has been used as an indicator of enhanced upwelling (Anderson and Prell, 1993; Peeters et al., 2002; Kucera, 2007; Tedesco and Thunnell, 2003).

The Southeast Brazilian margin of the South Atlantic hosts small western boundary upwelling zones, which are the result of interactions among NE winds, instabilities of the Brazil Current (BC) flow, and abrupt changes in the orientation of the continental margin (Gaeta et al., 1999; Rodrigues and Lorenzetti, 2001; Calado et al., 2010; Belem et al., 2013; Campos et al., 2013). Nonetheless, long-term evolution of this upwelling system is rather underexplored. In this study, we employed abundances of planktonic foraminifera and paleotemperature reconstructions at the upper (10 m) and lower (100 m) photic zone from a core at 24°S to detail upwelling occurrence in the SE Brazilian margin during two time intervals. These intervals comprise Marine Isotope Stage (MIS) 6 - 5 (140–75 kyr BP), and MIS 2 - 1 (20–6 kyr BP). The choice for studying a core at 24°S (Santos Basin) was to test the hypothesis that the SE Brazilian shelf upwelling systems expanded offshore, as seen by Portilho-Ramos et al. (2015) and Petró et al. (2016) at 21°S (Campos Basin), suggesting a large-scale upwelling system. In addition, our new data shows that expanded upwelling system was not a general interglacial feature since it is absent in the present. Different from the present interglacial, the last interglacial (MIS 5e) presented a distinct orbital variation, which intensified favorable oceanographic and atmospheric settings promoting the expansion of the upwelling.

2. Regional settings

Surface currents and vertical temperature distribution of the Southeast Brazilian continental margin (20–28°S) encompassing the Campos (20–23°S) and Santos (23–28°S) basins are shown in Fig. 1. The surface layer (0–200 m) is characterized by the warm and oligotrophic Tropical Water (TW), with temperatures between 18 and 27 °C and salinity above 36 (da Silveira et al., 2000). The presence of the TW in the photic zone of the BC maintains high sea surface temperatures (SST) and the thermocline below 200 m, thereby limiting productivity. The South Atlantic Central Water (SACW), formed in the Brazil–Malvinas Confluence zone at 38°S (in the vicinity of the mouth of the River Plata), flows in the thermocline layer. The SACW sinks and flows beneath the TW in the Subtropical front at 200–800 m, recirculates in the Subtropical Gyre, and is incorporated into the BC at 20°S (Stramma and England, 1999). The SACW has a temperature range of 6–18 °C and a salinity range of 34.5–36 (da Silveira et al., 2000). The SACW is the water mass responsible for high productivity events in the SE Brazilian margin where it upwells into the photic zone.

Despite the predominant oligotrophic scenario of the subtropical western South Atlantic, some important shelf upwelling zones occur along the Southeast Brazilian continental shelf (Fig. 1), including: (1) Vitória Upwelling System at 20°S generated through the cyclonic Vitória Eddy that is formed by friction between the BC and Abrolhos Bank (Schmid et al., 1995; Gaeta et al., 1999; Arruda et al., 2013); (2) Cabo de São Tomé (Calado et al., 2010); (3) the Cabo Frio Upwelling System (CFUS) between 22°–23°S that is the most important upwelling zone, presenting a high biological productivity zone encompassing the neritic realm (Valentin, 1984; Albuquerque et al., 2014); and, (4) the Cabo de Santa Marta Upwelling System at 28°S. These upwelling systems are favored by the topography of the continental margin and interactions with NE winds that promote BC instabilities and wind stress curl along the continental shelf. Those features induce SACW upwelling either on the coast and shelf or on the shelf break (Campos et al., 2000; Castella and Barth, 2006; Campos et al., 2013; Belem et al., 2013; Aguiar et al.,

2014).

The CFUS has provided data for most of the paleo-reconstructions of Brazilian upwelling zones, including assemblages of planktonic foraminifera. The CFUS is located on the continental shelf near the site of our core GL-1090 and, therefore, it can be used as a control area to evaluate variations in upwelling in relation to our reconstructions using the planktonic foraminifera assemblage. In areas adjacent to the CFUS, the relative abundance of *G. bulloides* remained below 5% throughout the Holocene and the last deglacial (Toledo et al., 2008; Lessa et al., 2014; Portilho-Ramos et al., 2015). However, within the CFUS, the relative abundance of *G. bulloides* during the Holocene reached values of up to $14 \pm 3\%$ for specimens of $> 125 \mu\text{m}$ and values of up to $18 \pm 5\%$ for specimens $> 150 \mu\text{m}$ (Lessa et al., 2014, 2016). These values are close to those of important eastern boundary upwelling systems such as the Humboldt, Mauritania and Benguela (20–40%) and the SW Indonesia (15–30%) currents (Giraudeau et al., 1993; Kucera et al., 2005; Mohtadi et al., 2005, 2007).

3. Material and methods

The sediment core GL-1090 (Fig. 1) was collected by Petrobras in the Santos Basin slope (24.92°S, 42.51°W) in a water depth of 2225 m, recovering a sediment column of 19.14 m. The core GL-1090 covers a time range from 185 to 6 kyr and its mean sedimentation rate is 13 cm/kyr with the lowest values occurring during interglacials (MIS 5e and MIS 1) and highest values during MIS 4. The age model of core GL-1090 was described in details in Santos et al. (2017).

The planktonic foraminifera assemblage was defined for core sections representing ages from 140 to 75 kyr BP (MIS 6 and MIS 5) and from 20 to 5 kyr BP (MIS 2 and MIS 1). We analyzed assemblages with 4 cm resolution for MIS 1 and 5e sections due to low sedimentation rate, and 10 cm for the other sections. We washed 10 cm³ of sediment through a 150 μm mesh sieve and the residue was dried at 50 °C for 24 h. The fraction $> 150 \mu\text{m}$ was re-sieved dry and then divided until 300–500 individuals remained for identification at species level. Species were identified according to Kennett and Srinivasan (1983) and Loeblich and Tappan (1988). Individuals identified as *Globigerina bermudezi* (e.g. Vicalvi, 1997) were classified as *G. bulloides* since the single difference between them is the occurrence of one or two big *kummerform* chambers in *G. bermudezi* tests. However, *G. bermudezi* individuals were always much rarer than *G. bulloides* sensu stricto individuals. We did not consider the influence of dissolution on the assemblage's composition or for our paleoceanographic interpretations since core GL-1090 was collected from a depth above the lysocline (Van Andel et al., 1977).

Using census counts of planktonic foraminifera, we calculated the relative abundances of *Globigerinoides ruber* white (TW dwelling) and *G. bulloides* (related to upwelling-driven high productivity) and we estimated paleotemperatures with the whole assemblage through the Modern Analog Technique (MAT) (Hutson, 1980). To do that, we used the MARGO project databank of 891 core tops with planktonic foraminifera assemblages and temperature values from the entire Atlantic (Kucera et al., 2005). We chose to use the entire Atlantic database rather than the South Atlantic database alone due to a lack of South Atlantic analogs between 5 and 15 °C and because both reconstructed temperature variations and noise were similar in both developed models. In addition, 161 core tops from upwelling areas off Iberian Peninsula and NW Africa (Salgueiro et al., 2014) were added to data base aiming to increase the number of analogs for upwelling conditions. Temperature values were extracted for each core top in two water column layers (10 and 100 m) from the World Ocean Atlas (WOA) 2013 (Boyer et al., 2013) using the Ocean Data View software (Schlitzer, 2014). The choice of temperatures at 10 and 100 m is referent to upper and lower limits of the photic zone and it allows us visualize the potential influence of SACW upwelling over the maximum primary productivity layers. The MAT method is based on calculations of

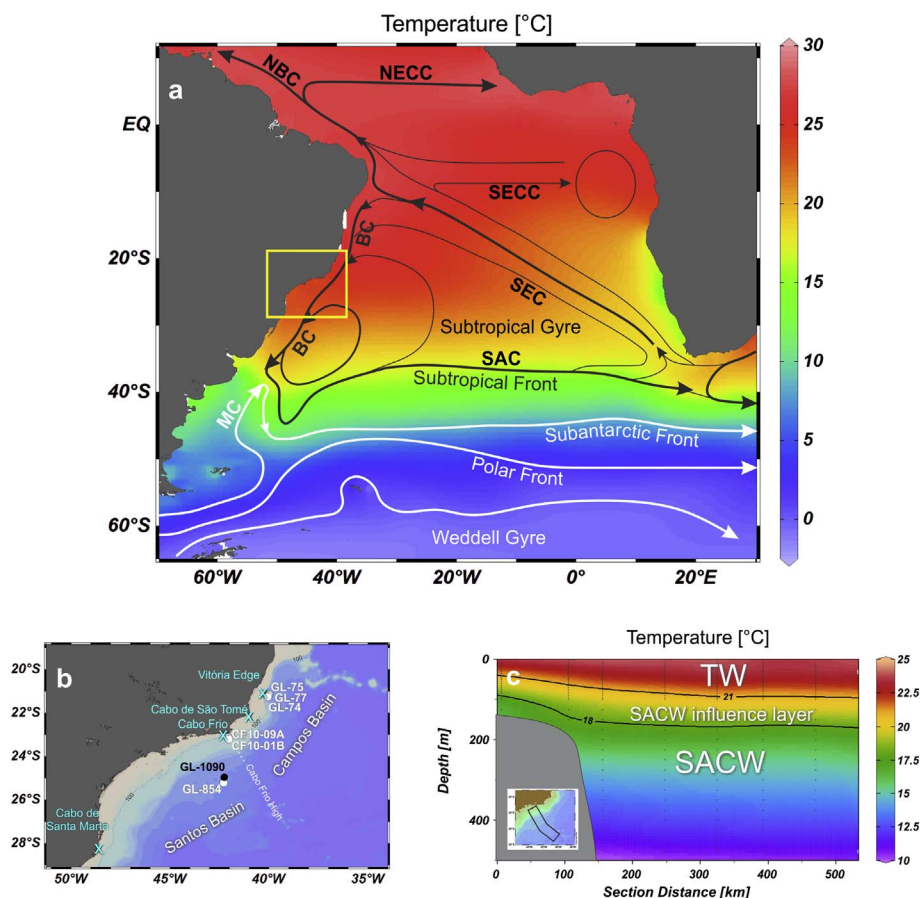


Fig. 1. (a) Map of the South Atlantic surface circulation (modified from Peterson and Stramma, 1991) and the SST spatial distribution. (b) View of the study area (yellow rectangle in (a)) showing the bathymetry (filling) highlighting the 100 m isobath, location of core GL-1090 used in this study (black circle) and cores from Santos (24°S) and Campos (21°S) basins used for comparison (Portilho-Ramos et al., 2015; Petró et al., 2016; Lessa et al., 2014, 2016; Almeida et al., 2015) (white circles), as well as current upwelling zones (cyan crosses). (c) Vertical distribution of the temperature in the first 450 m depth of the Santos Basin transect (small map) showing the water masses (separated by the 18 °C isotherm, according to Albuquerque et al., 2014) responsible for coastal and shelf upwelling events. Acronyms: SEC – South Equatorial Current; SECC – South Equatorial Countercurrent; NBC – North Brazil Current; NECC – North Equatorial Countercurrent; BC - Brazil Current; SAC – South Atlantic Current; MC – Malvinas (Falkland) Current; TW – Tropical Water; SACW – South Atlantic Central Water. (For interpretation of the references to color in this figure legend, the reader is referred to the web version of this article.)

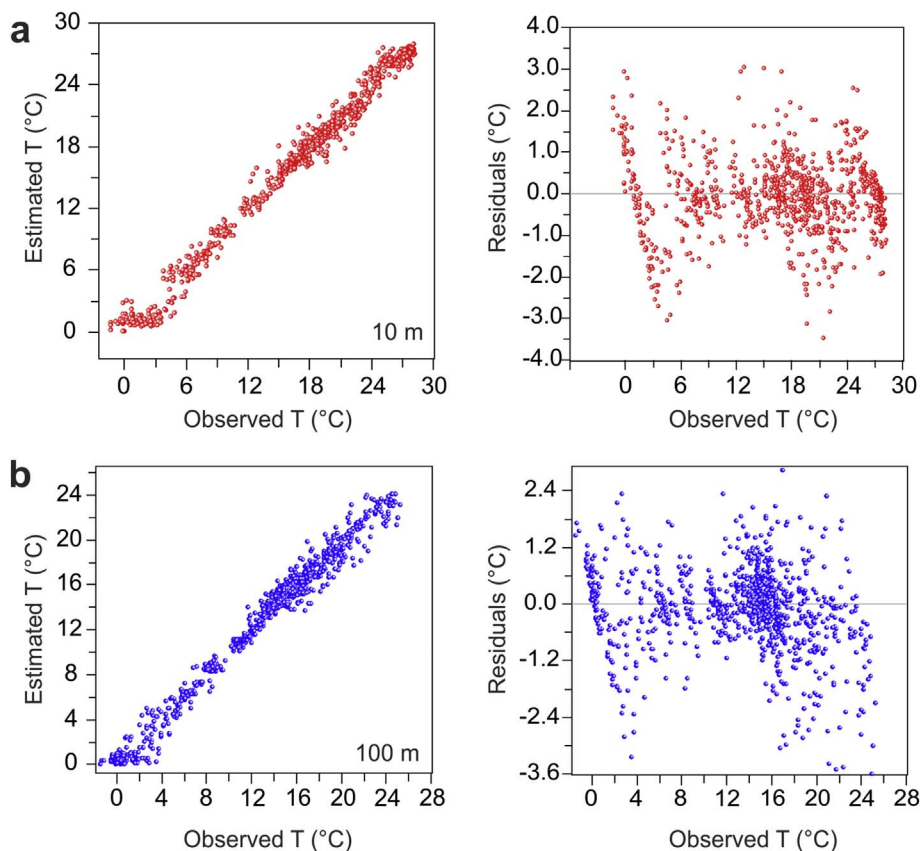


Fig. 2. Graphical modeling of the MAT method for paleotemperature reconstruction showing the correlation and residuals between observed and estimated temperatures at 10 m (a), and 100 m (b) using the core-tops foraminifera databank (North and South Atlantic) from Kucera et al. (2005) and Salgueiro et al. (2008, 2014). Numerical data on model performances are summarized in Table 1.

Table 1
MAT performance for temperature reconstructions for two targeted water depths using leave-one-out cross-validation.

Model	R ²	RMSEP (°C)	Average bias (°C)	Maximum bias (°C)
Temperature 10 m	0.990	0.850	0.053	1.008
Temperature 100 m	0.980	0.893	0.0903	1.019

dissimilarity between the downcore assemblage (fossil) and the core-tops data base (Hutson, 1980). We performed the MAT method in the C2 software (Juggins, 2003), and performance of the models in reconstructing paleotemperatures was cross-validated using the *leave one out* method. Analogs dissimilarity was calculated using the *Square Chord* distance and the estimated paleotemperature was obtained by the weighted mean from the 10 best core-top analogs. Graphical and numeric representations of model performances are summarized in Fig. 2 and Table 1.

4. Results

Estimated temperatures at 10 m (T_{10m}) ranged between 21.5 and 27 °C (Fig. 3), with low values between 140 and 120 kyr BP and high values during MIS 5c, 5a and during the last 20 kyr. Estimated temperatures at 100 m (T_{100m}) ranged between 15.8 and 23.5 °C and variations exhibited the opposite trend to the surface layer, except after 10 kyr BP. For T_{100m} , values were high during MIS 6, 5a and most of the last 20 kyr. Low values ranged from MIS 5e to Early MIS 5c and at about 15 kyr BP.

The relative abundance of *G. ruber* white ranged between 18 and 63% (average $36.2 \pm 8.48\%$) (Fig. 3). The highest percentages occurred between 90 and 80 kyr BP (MIS 5b) and after 20 kyr BP. The lowest percentages occurred during the MIS 5e and 5d (130 and 110 kyr BP). The relative abundance of *G. bulloides* ranged between 0.4 and 28% (average $10.5 \pm 7.25\%$), with the highest values occurring from the end of the penultimate deglacial to MIS 5c (130–98 kyr BP), which were generally within or above the CFUS average Holocene range. Low percentages of *G. bulloides* occurred after 20 kyr BP.

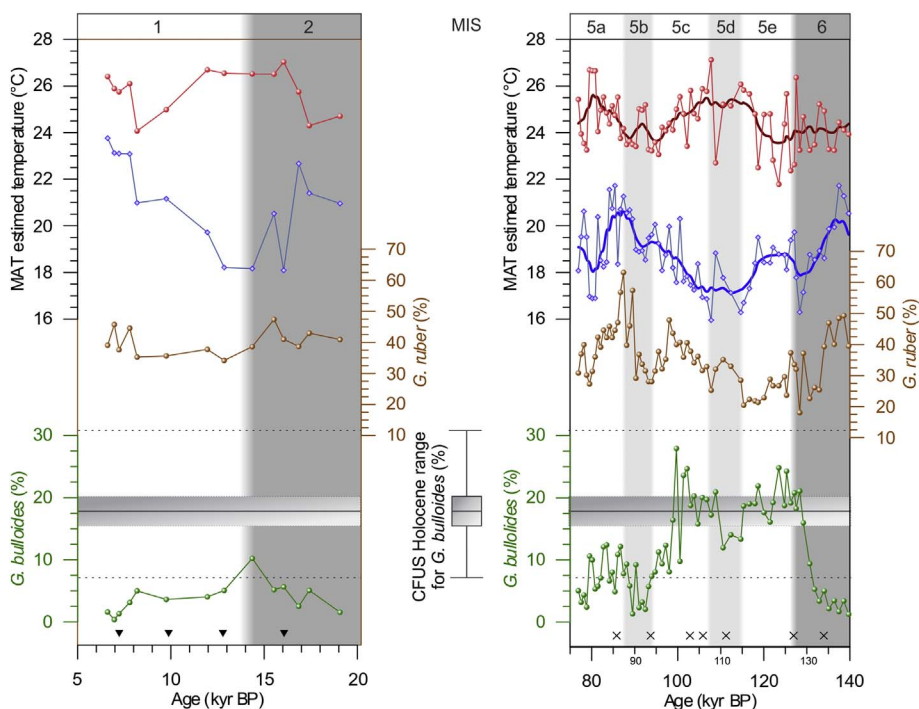


Fig. 3. Estimated paleotemperatures by MAT at depths of 10 m (red) and 100 m (blue) with a 7 points weighted running mean to MIS 5 (thick lines). Relative abundances of *G. ruber* white (brown; a Tropical Water indicator) and *G. bulloides* (green; an upwelling indicator) along the MIS 5 and the last 20 kyr of core GL-1090. Marine isotopic stages (MIS) are partitioned into white and light grey subdivisions. Triangles (along X-axis of left panel) indicate ¹⁴C AMS-dated ages and crosses (along X-axis of right panel) indicate chosen benthic foraminifera ¹⁸O tie-points according to Santos et al. (2017). Boxplot shows *G. bulloides* abundance variation at Cabo Frio Upwelling System (CFUS) during the Holocene (size fraction > 150 μm; solid line and grey band represent recent mean and standard deviation (Lessa et al., 2014); dotted lines represent Holocene maximum and minimum values (Lessa et al., 2016)).

5. Discussion

The relative abundance of *G. bulloides* has been used as an upwelling indicator in several studies (Little et al., 1997a; Marchant et al., 1999; Anderson and Prell, 1993; Lessa et al., 2014). In the CFUS and adjacent areas, Lessa et al. (2014) described the distribution of *G. bulloides* between the Campos and Santos basins and showed that high abundances of this species occur only in the CFUS (up to 15%). Considering only > 150 μm sized individuals in the assemblage of that study, the average relative abundance of *G. bulloides* increased up to 18%. Overall, that study indicated that relative abundance values $\geq 15\%$ can be linked to upwelling conditions in the SE Brazilian margin. The relative abundance values of *G. bulloides* for the CFUS are similar to those reported in eastern boundary upwelling systems such as the Humboldt, Mauritania and Benguela (20–40%) and the SW Indonesia (15–30%) systems (Giraudeau et al., 1993; Kucera et al., 2005; Mohtadi et al., 2005, 2007). Therefore, we compared the range of *G. bulloides* relative abundance in the CFUS (Lessa et al., 2014, 2016) during the Holocene to our *G. bulloides* relative abundance values from core GL-1090 to identify and evaluate periods of expansion of the coastal upwelling zones. In addition, we used a ratio between *G. bulloides* and *G. ruber* white (Gb/Gr) to verify changes in upwelling intensity during high-intensity periods (Fig. 4). High Gb/Gr ratios suggest cold water intrusions in the surface layer, whereas low values suggest a predominance of warm surface waters (Conan et al., 2002; Toledo et al., 2008; Lessa et al., 2014; Lessa et al., 2016).

Our results for core GL-1090 indicate high relative abundances of *G. bulloides*, frequently above 20%, from MIS 5e to 5c that are comparable to values from the CFUS (Fig. 3). Such high values and the divergence between T_{10m} and T_{100m} indicate that our site at 24°S presented upwelling conditions similar to or stronger than the Holocene CFUS between 130 and 98 kyr BP. The presence of the SACW in the surface layer was at its maximum between 120 and 115 kyr BP, migrating to deeper layers towards MIS 4. In contrast, high abundances of *G. ruber* white, low Gb/Gr values, and high T_{10m} and T_{100m} indicated the predominance of the TW after 20 kyr BP (Figs. 3 and 4). After 20 kyr, the thermocline was likely deeper and the state of the BC was similar to nowadays, with a thick warm layer covering the entire photic zone that favored tropical and subtropical planktonic foraminifera species, such

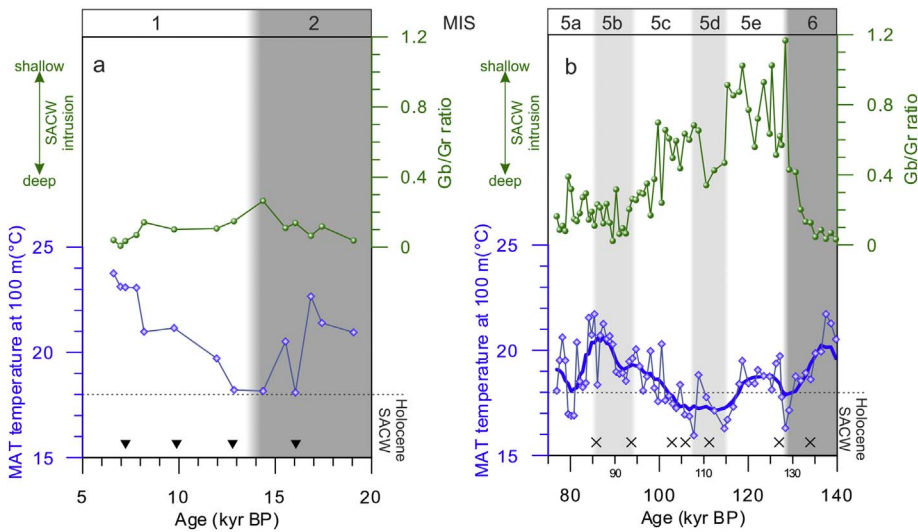


Fig. 4. Variation of the ratio between *G. bulloides* and *G. ruber* white (Gb/Gr) and the MAT temperature at 100 m along MIS 2 - 1 (a) and MIS 5 (b) GL-1090 core sections. Dotted lines indicate the Holocene TW-SACW boundary. Triangles indicate ^{14}C AMS-dated ages and crosses indicate benthic foraminifera $\delta^{18}\text{O}$ tie-points according to Santos et al. (2017).

as *G. ruber*. Thus, we assume that the modern foraminiferal assemblage was established at 20 kyr BP. The difference in foraminiferal assemblages between MIS 1 and MIS 5 found here and described in another study (Portilho-Ramos et al., 2015) is puzzling. Our results prompted us to consider that a warmer climate alone is insufficient to promote upwelling expansion.

In Fig. 5, we plot the observed variation in relative abundances of *G. bulloides* from Portilho-Ramos et al. (2015) and Petró et al. (2016) from Campos Basin (21°S) and our data from core GL-1090 (24°S) to investigate spatial expansion of the upwelling system along the western South Atlantic. The records at 21°S mirror our results at 24°S, i.e. they exhibit high relative abundances of *G. bulloides* during MIS 5 (exceeding the CFUS mean value of 20%) and values lower than the CFUS minimum after 20 kyr BP (Fig. 5). The concordance of these three datasets clearly reveals that a large-scale expansion of the upwelling system dominated most of MIS 5. Portilho-Ramos et al. (2015) attributed the high abundance of large *G. bulloides* specimens between 110 and 88 kyr BP to changes in coastline configuration due to a lower sea-level stand (20–70 m lower than today). This lower sea-level promoted greater instability of the BC when it passed the Abrolhos Bank, which favored upwelling of the SACW (Portilho-Ramos et al., 2015). If this reasoning was correct, during MIS 5e when the sea-level was 7 ± 12 m

higher than present (Thompson and Goldstein, 2005; Rohling et al., 2008; Spratt and Lisiecki, 2016), a low *G. bulloides* relative abundance should have been observed. However, our new data and that of Petró et al. (2016), exhibit a sharp increase in *G. bulloides* abundances with the onset of MIS 5e. Therefore, interglacial ocean-atmosphere dynamics should be invoked as the main factor responsible for this expanded upwelling system, and not sea-level fluctuations.

Since upwelling systems are generally wind-driven, insolation and orbital configurations may play an important role in intensifying or weakening wind systems over the long term (Little et al., 1997b; Peeters et al., 2004). MIS 5 is characterized by eccentricity values above 0.033, which are consistently higher than the eccentricity after 20 kyr BP (Fig. 5). The eccentricity maximum during MIS 5 boosted the precessional amplitude, leading to a stronger seasonal modulation of insolation. Thus, these high eccentricity values would have influenced the wind regime at our study site by controlling the amplitude of the winter and summer insolation and, as a consequence, altering seasonality (Fischer and Jungclauss, 2010; Bakker et al., 2014; Kostadinov and Gilb, 2014). Warmer summers during MIS 5 would have induced stronger NE winds, which are fundamental to contemporary continental shelf upwelling in this region. Model simulations comparing MIS 5e and pre-industrial periods revealed a warmer and drier climate in Brazil and the

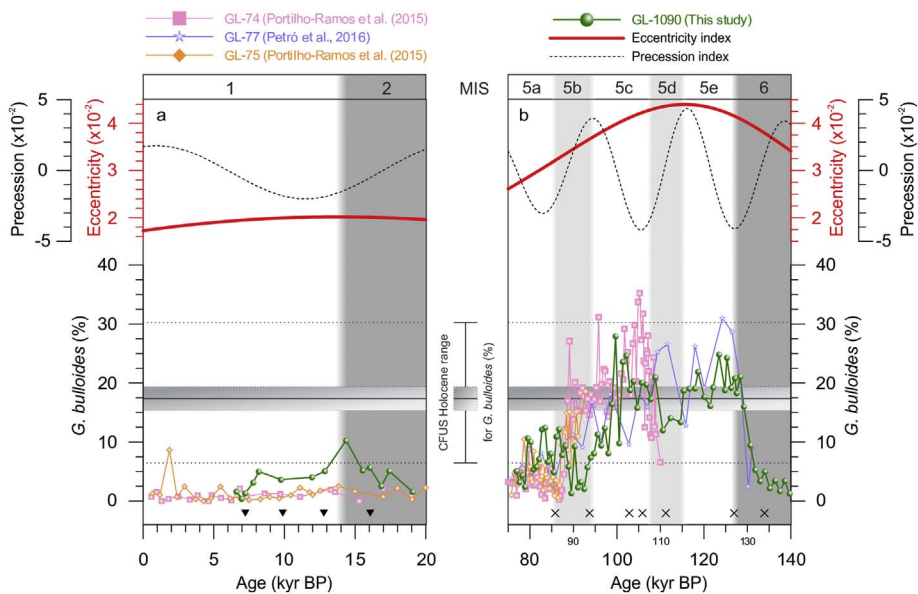


Fig. 5. Comparison of orbital parameters (extracted from Berger and Loutre, 1991) and *G. bulloides* relative abundances in 21°S cores (Portilho-Ramos et al., 2015; Petró et al., 2016) and a 24°S core (GL-1090, this study) along the (a) last 20 kyr and (b) MIS 5 core sections. The boxplot shows the range of *G. bulloides* relative abundance for the Holocene at the CFUS (Lessa et al., 2014, 2016). Triangles indicate ^{14}C AMS-dated ages and crosses indicate benthic foraminifera $\delta^{18}\text{O}$ tie-points according to Santos et al. (2017).

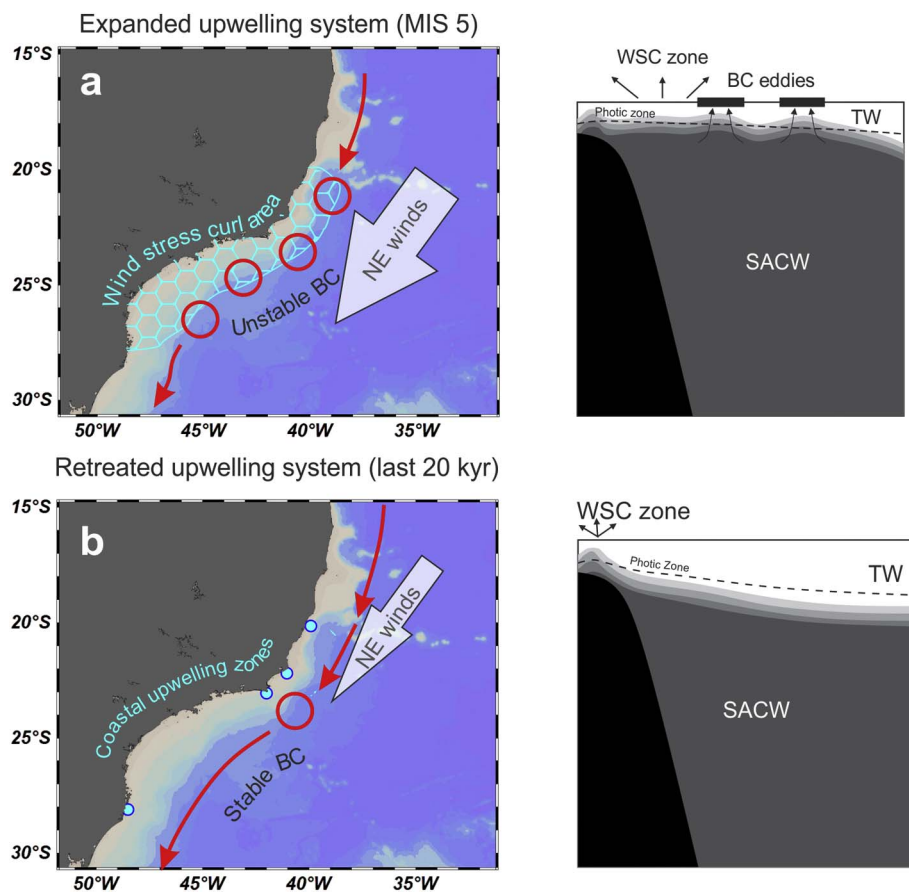


Fig. 6. Conceptualization of the Southwest Subtropical Atlantic surface circulation for MIS 5 (a) and after 20 kyr BP (b), highlighting the favorable oceanographic and atmospheric factors for expansion and retreat of the upwelling system, with spatial (left) and vertical (right) views. Dashed lines in panels at right indicate the photic zone boundary. WSC = wind stress curl.

western South Atlantic during MIS 5e (Fischer and Jungclauss, 2010). These simulations suggested a westward displacement of the South Atlantic high pressure system during the Last Interglacial, which consequently reduced the moisture and increased the air temperature over South America. This reasoning could be applied to most of MIS 5, since not only MIS 5e presented high eccentricity values (Fig. 5). Considering that the NE winds represent the western border of the South Atlantic high pressure system, more prolonged NE wind episodes might have been common in our study area during MIS 5 summers. In contrast, the eccentricity values below 0.002 might not have been able to enhance NE winds and bring the South Atlantic high-pressure system near enough to the continental margin to promote expansion of the upwelling zone after 20 kyr BP (Fig. 5).

Fig. 6 and Table 2 summarize the contrasting conditions between 140 and 75 kyr BP and 20–6 kyr BP. The upwelling intensification observed during MIS 5 led to a shoaling of the 18 °C isotherm (which represents the present-day TW-SACW boundary, Belem et al., 2013), driving the nutrient-rich SACW into the photic zone (Fig. 6a). During the last 20 kyr BP, the upwelling system weakened and offshore waters presented low productivity (Fig. 6b). With a more stable BC flux in the last 20 kyr BP, the SACW rarely reached the photic zone in offshore

areas, restricting high productivity areas to current shelf upwelling zones. Therefore, we suggest that an expanding–retreating upwelling system is likely located between the latitudes of 20°S and 28°S. This spatial range is based on the locality where modern continental shelf upwelling zones are observed (Fig. 1). Therefore, the CFUS and other upwelling zones along the Brazilian continental margin are modern remnants of this more extensive system.

Besides the SE Brazilian margin, strong upwelling events during MIS 5 have also been documented for the Arabian monsoonal upwelling system (Leuschner and Sirocko, 2003; Ishikawa and Oda, 2007). The similarities between these two western oceanic boundary areas indicate that the wind regime of low latitudes is an important regulator of upwelling dynamics at these locations. In addition, more broadly, i.e. encompassing both the Indian and South Atlantic basins, the wind regime could determine oligotrophic or eutrophic conditions in both the western South Atlantic and western Indian basins. Based on our new results, we suggest that a close relationship exists between variations in the amplitude of eccentricity and offshore expansions of upwelling systems between the latitudes of 20 and 28°S. However, more studies with a wider time range and atmospheric modeling in the South Atlantic are necessary to confirm or refute our hypothesis. We also

Table 2
Summary of the reconstructed interglacial scenarios in the Southwest Subtropical Atlantic (SWSA) upwelling system.

SWSA upwelling system	Time	Main characteristics
Expanded mode	MIS 5 (130–90 kyr BP)	<ul style="list-style-type: none"> ● Intense wind regime due to enhanced summer signal (high eccentricity) ● Unstable BC flux combined with wind stress curl on shelf and coastal Ekman transport. ● Shallow offshore thermocline due to BC instabilities.
Retreated mode	Last 20 kyr BP	<ul style="list-style-type: none"> ● Reduced summer signal (low eccentricity) ● More stable BC flux, so upwelling restricted to shelf zones. ● Offshore thermocline below the photic zone.

highlight that future studies using proxies related to the carbon cycle (e.g. stable isotopes of carbon and boron) could generate valuable insights into the consequences of this expansion of upwelling systems in terms of the carbon budget during MIS 5.

6. Conclusions

Using relative abundance of *G. bulloides* and temperature reconstructions from core GL-1090, we observed intense upwelling events in the Santos Basin (24°S) during MIS 5. The agreement between several marine records suggests that current coastal upwelling zones are remnants of a larger expanding–retreating western boundary upwelling system that spanned 20 to 28°S of the SE Brazilian continental margin. This upwelling system was characterized by the presence of the TW in the uppermost layer, while the deep photic layer was dominated by intrusions of the SACW associated with prolonged episodes of intense NE winds. We suggest that variation in seasonal amplitude, modulated by eccentricity, was the dominant factor contributing to upwelling system expansion during MIS 5 and retreat after 20 kyr BP.

Acknowledgments

Funding: This study was supported by CAPES/Paleocean project (23038.001417/2914-71) and by CNPq/PDJ program (157272/2015-0). CNPq financially supported IMV with a scholarship from the CsF (“Cienciasem Fronteiras”) project (grant 248819/2013-5). ALA is a CNPq senior researcher (grant 306385/2013-9).

We thank Petrobras for providing the sediment core employed in this research. The data reported in this paper will be archived in Pangaea (www.pangaea.de). We thank Rodrigo Portilho Ramos for providing *G. bulloides* data from GL-74 and GL-75 and the Kucera et al. (2005) Atlantic database for MAT analysis. We thank Renato Kowsman (CENPES/Petrobras) who made important contributions during manuscript preparation. Finally, the authors thank Dr. Antje Voelker and an anonymous reviewer for their important contributions to the improvement of the manuscript.

References

- Abrantes, F., 1991. Increased upwelling off Portugal during the last glaciation: diatom evidence. *Mar. Micropaleontol.* 17, 285–310.
- Abrantes, F., 1992. Paleoproductivity oscillations during the last 130 ka along the Portuguese and NW African margins. In: Summerhayes, C.P., Prell, W.L., Emeis, K.C. (Eds.), *Upwelling Systems: Evolution Since the Early Miocene*. The Geological Society, London, pp. 499–510.
- Aguiar, A.L., Cirano, M., Pereira, J., Marta-Almeida, M., 2014. Upwelling processes along a western boundary current in the Abrolhos–Campos region of Brazil. *Cont. Shelf Res.* 85, 42–59.
- Albuquerque, A.L.S., et al., 2014. Particle fluxes and bulk geochemical characterization of the Cabo Frio upwelling system in Southeastern Brazil: sediment trap experiments between Spring 2010 and Summer 2012. *An. Acad. Bras. Cienc.* 86 (2), 601–620.
- Almeida, F.K., Mello, R.M., Costa, K.B., Toledo, F.A.L., 2015. The response of deep-water benthic foraminiferal assemblages to changes in paleoproductivity during the Pleistocene (last 769.2 kyr), western South Atlantic Ocean. *Palaeogeogr. Palaeoclimatol. Palaeoecol.* 440, 201–212.
- Anderson, D.M., Prell, W.L., 1993. A 300 KYR record of upwelling off Oman during the Late Quaternary: evidence of the Asian Southwest Monsoon. *Paleoceanography* 8 (2), 193–208.
- Arruda, W.Z., Campos, E.J.D., Zharkov, V., Soutelino, R.G., da Silveira, I.C.A., 2013. Events of equatorward translation of the Vitoria Eddy. *Cont. Shelf Res.* 70, 61–73.
- Bakker, P., et al., 2014. Temperature trends during the Present and Last Interglacial periods—a multi-model-data comparison. *Quat. Sci. Rev.* 99, 224–243.
- Bakun, A., 1990. Global climate change and intensification of coastal ocean upwelling. *Science* 247 (4939), 198–201.
- Belem, A.L., Castela, R.M., Albuquerque, A.L., 2013. Controls of subsurface temperature variability in a western boundary upwelling system. *Geophys. Res. Lett.* 40 (7), 1362–1366.
- Berger, A., Loutre, M.F., 1991. Insolation values for the climate of the last 10 million years. *Quat. Sci. Rev.* 10 (4), 297–317.
- Boyer, T.P., et al., 2013. In: Levitus, S., Mishonov, A. (Eds.), *World Ocean Database 2013*, NOAA Atlas NESDIS 72, Technical Ed. Silver Spring, MD (209 pp).
- Calado, L., da Silveira, I.C.A., Gangopadhyay, A., de Castro, B.M., 2010. Eddy-induced upwelling off Cape São Tomé (22°S, Brazil). *Cont. Shelf Res.* 30 (10–11), 1181–1188.
- Campos, E.J.D., Velhote, D., da Silveira, I.C.A., 2000. Shelf break upwelling driven by Brazil Current cyclonic meanders. *Geophys. Res. Lett.* 27 (6), 751–754.
- Campos, P.C., Möller, O.O., Piola, A.R., Palma, E.D., 2013. Seasonal variability and coastal upwelling near Cape Santa Marta (Brazil). *J. Geophys. Res. Oceans* 118 (3), 1420–1433.
- Castela, R.M., Barth, J.A., 2006. Upwelling around Cabo Frio, Brazil: the importance of wind stress curl. *Geophys. Res. Lett.* 33 (3), L03602.
- Conan, S.M.H., Ivanova, E.M., Brummer, G.J.A., 2002. Quantifying carbonate dissolution and calibration of foraminiferal dissolution indices in the Somali Basin. *Mar. Geol.* 182, 325–349.
- Fischer, N., Jungclauss, J.H., 2010. Effects of orbital forcing on atmosphere and ocean heat transports in Holocene and Eemian climate simulations with a comprehensive Earth system model. *Clim. Past* 6, 155–168.
- Gaeta, S., et al., 1999. The Vitória Eddy and its relation to the phytoplankton biomass and primary productivity during the austral fall of 1995. *Arch. Fishery Mar. Res.* 47 (2–3), 253–270.
- Giraudeau, J., Monteiro, P.M.S., Nikodemus, K., 1993. Distribution and malformation of living coccolithophores in the northern Benguela upwelling system off Namibia. *Mar. Micropaleontol.* 22 (1), 93–110.
- Heymans, J.J., Baird, D., 2000. A carbon flow model and network analysis of the northern Benguela upwelling system, Namibia. *Ecol. Model.* 126 (1), 9–32.
- Hutson, W.H., 1980. The Agulhas Current during the Late Pleistocene: analysis of modern faunal analogs. *Science* 207 (4426), 64–66.
- Ishikawa, S., Oda, M., 2007. Reconstruction of Indian monsoon variability over the past 230,000 years: planktic foraminiferal evidence from the NW Arabian Sea open-ocean upwelling area. *Mar. Micropaleontol.* 63 (3), 143–154.
- Juggins, S., 2003. *Software for Ecological and Palaeoecological Data Analysis and Visualisation*. User Guide Version. 1. pp. 5. <http://www.staff.ncl.ac.uk/stephen.juggins>.
- Kennett, J.P., Srinivasan, M., 1983. *Neogene Planktonic Foraminifera: A Phylogenetic Atlas*. Hutchinson Ross, Stroudsburg (273 pp).
- Kim, J.-H., Schneider, R.R., Mulitza, S., Müller, P.J., 2003. Reconstruction of SE trade-wind intensity based on sea-surface temperature gradients in the Southeast Atlantic over the last 25 kyr. *Geophys. Res. Lett.* 30 (22), 2144.
- Kostadinov, T.S., Gilb, R., 2014. Earth Orbit v2.1: a 3-D visualization and analysis model of Earth's orbit, Milankovitch cycles and insolation. *Geosci. Model Dev.* 7 (3), 1051–1068.
- Kucera, M., 2007. Planktonic foraminifera as tracers of past oceanic environments. In: Claude, H.M., Anne De, V. (Eds.), *Developments in Marine Geology: Proxies in Late Cenozoic Paleoclimatology*. Elsevier, Montreal, pp. 213–262.
- Kucera, M., et al., 2005. Reconstruction of sea-surface temperatures from assemblages of planktonic foraminifera: multi-technique approach based on geographically constrained calibration data sets and its application to glacial Atlantic and Pacific Oceans. *Quat. Sci. Rev.* 24 (7–9), 951–998.
- Lessa, D.V.O., et al., 2014. Planktonic foraminifera in the sediment of a western boundary upwelling system off Cabo Frio, Brazil. *Mar. Micropaleontol.* 106, 55–68.
- Lessa, D.V., et al., 2016. Holocene oscillations of Southwest Atlantic shelf circulation based on planktonic foraminifera from an upwelling system (off Cabo Frio, Southeastern Brazil). *The Holocene* 26 (8), 1175–1187.
- Leuschner, D.C., Sirocko, F., 2003. Orbital insolation forcing of the Indian Monsoon—a motor for global climate changes? *Palaeogeogr. Palaeoclimatol. Palaeoecol.* 197 (1), 83–95.
- Little, M.G., et al., 1997a. Rapid palaeoceanographic changes in the Benguela Upwelling System for the last 160,000 years as indicated by abundances of planktonic foraminifera. *Palaeogeogr. Palaeoclimatol. Palaeoecol.* 130 (1–4), 135–161.
- Little, M.G., et al., 1997b. Trade wind forcing of upwelling, seasonality, and Heinrich events as a response to sub-Milankovitch climate variability. *Paleoceanography* 12 (4), 568–576.
- Loeblich, A., Tappan, H., 1988. *Foraminiferal Genera and Their Classification*. 2. van Nostrand Reinhold Company Publisher, pp. 1–212.
- Marchant, M., Hebbeln, D., Wefer, G., 1999. High resolution planktic foraminiferal record of the last 13,300 years from the upwelling area off Chile. *Mar. Geol.* 161 (2–4), 115–128.
- Matsuzaki, K.M.R., et al., 2011. Paleoclimatology of the Mauritanian margin during the last two climatic cycles: from planktonic foraminifera to African climate dynamics. *Mar. Micropaleontol.* 79 (3), 67–79.
- Mohtadi, M., Hebbeln, D., Marchant, M., 2005. Upwelling and productivity along the Peru–Chile Current derived from faunal and isotopic compositions of planktic foraminifera in surface sediments. *Mar. Geol.* 216 (3), 107–126.
- Mohtadi, M., et al., 2007. Modern environmental conditions recorded in surface sediment samples off W and SW Indonesia: planktonic foraminifera and biogenic compounds analyses. *Mar. Micropaleontol.* 65 (1–2), 96–112.
- Muller-Karger, F., et al., 2001. Annual cycle of primary production in the Cariaco Basin: response to upwelling and implications for vertical export. *J. Geophys. Res. Oceans* 106 (C3), 4527–4542.
- Narayan, N., Paul, A., Mulitza, S., Schulz, M., 2010. Trends in coastal upwelling intensity during the late 20th century. *Ocean Sci.* 6 (3), 815.
- Pauly, D., Christensen, V., 1995. Primary production required to sustain global fisheries. *Nature* 374 (6519), 255–257.
- Peeters, F.J.C., Brummer, G.-J.A., Ganssen, G., 2002. The effect of upwelling on the distribution and stable isotope composition of *Globigerina bulloides* and *Globigerinoides ruber* (planktic foraminifera) in modern surface waters of the NW Arabian Sea. *Glob. Planet. Chang.* 34 (3–4), 269–291.
- Peeters, F.J.C., et al., 2004. Vigorous exchange between the Indian and Atlantic oceans at the end of the past five glacial periods. *Nature* 430 (7000), 661–665.
- Peterson, R.G., Stramma, L., 1991. Upper-level circulation in the South Atlantic Ocean.

- Prog. Oceanogr. 26, 1–73.
- Petró, S.M., Pivel, M.A.G., Coimbra, J.C., 2016. Paleooceanographic changes through the last 130 ka in the Western South Atlantic based on planktonic foraminifera. *Revista Brasileira de Paleontologia* 19 (1), 3–14.
- Portilho-Ramos, R.C., Ferreira, F., Calado, L., Frontalini, F., de Toledo, M.B., 2015. Variability of the upwelling system in the southeastern Brazilian margin for the last 110,000 years. *Glob. Planet. Chang.* 135, 179–189.
- Rodrigues, R.R., Lorenzetti, J.A., 2001. A numerical study of the effects of bottom topography and coastline geometry on the Southeast Brazilian coastal upwelling. *Cont. Shelf Res.* 21 (4), 371–394.
- Rohling, E.J., et al., 2008. High rates of sea-level rise during the last interglacial period. *Nat. Geosci.* 1 (1), 38–42.
- Romero, O.E., Kim, J., Donner, B., 2008. Submillennial-to-millennial variability of diatom production off Mauritania, NW Africa, during the last glacial cycle. *Paleoceanography* 23, PA3218.
- Salgueiro, E., et al., 2008. Planktonic foraminifera from modern sediments reflect upwelling patterns off Iberia: insights from a regional transfer function. *Mar. Micropaleontol.* 66 (3), 135–164.
- Salgueiro, E., et al., 2014. Past circulation along the western Iberian margin: a time slice vision from the Last Glacial to the Holocene. *Quat. Sci. Rev.* 106, 316–329.
- Santos, T.P., et al., 2017. Prolonged warming of the Brazil Current precedes deglaciations. *Earth Planet. Sci. Lett.* 463, 1–12.
- Schlitzer, R., 2014. **Ocean Data View**. Available from: <http://odv.awi.de>.
- Schmid, C., Schäfer, H., Zenk, W., Podestá, G., 1995. The Vitória Eddy and its relation to the Brazil Current. *J. Phys. Oceanogr.* 25 (11), 2532–2546.
- da Silveira, I.C.A., Schmidt, A.C.K., Campos, E.J.D., de Godoi, S.S., Ikeda, Y., 2000. A corrente do Brasil ao largo da costa leste brasileira. *Rev. Bras. Oceanogr.* 48, 171–183.
- Spratt, R.M., Lisiecki, L.E., 2016. A Late Pleistocene sea level stack. *Clim. Past* 12 (4), 1079–1092.
- Stramma, L., England, M., 1999. On the water masses and mean circulation of the South Atlantic Ocean. *J. Geophys. Res.* 104 (C9), 20863–20883.
- Tedesco, K.A., Thunell, R.C., 2003. Seasonal and interannual variations in planktonic foraminiferal flux and assemblage composition in the Cariaco Basin, Venezuela. *J. Foraminiferal Res.* 33 (3), 192–210.
- Thiel, M., et al., 2007. The Humboldt Current System of northern and central Chile: oceanographic processes, ecological interactions and socioeconomic feedback. *Oceanogr. Mar. Biol.* 45, 195–344.
- Thompson, W.G., Goldstein, S.L., 2005. Open-system coral ages reveal persistent sub-orbital sea-level cycles. *Science* 308 (5720), 401–404.
- Thunell, R., Sautter, L.R., 1992. Planktonic foraminiferal faunal and stable isotopic indices of upwelling: a sediment trap study in the San Pedro Basin, Southern California Bight. In: Summerhayes, C.P., Prell, W.L., Emeis, K.C. (Eds.), *Upwelling Systems: Evolution Since the Early Miocene*. The Geological Society Special Publication, London, pp. 77–91.
- Toledo, F.A., Costa, K.B., Pivel, M.A., Campos, E.J., 2008. Tracing past circulation changes in the western South Atlantic based on planktonic foraminifera. *Revista Brasileira de Paleontologia* 11 (3), 169–178.
- Valentin, J.L., 1984. Analyse des paramètres hydrobiologiques dans la remontée de Cabo Frio (Brésil). *Mar. Biol.* 82 (3), 259–276.
- Van Andel, T.H., et al., 1977. Depositional history of the South Atlantic Ocean during the last 125 million years. *J. Geol.* 85 (6), 651–698.
- Vivalvi, M.A., 1997. Zoneamento bioestratigráfico e paleoclimático dos sedimentos do Quaternário superior do talude da Bacia de Campos, RJ, Brasil. *Boletim de Geociências da PETROBRAS* 11 (1/2), 132–165.
- Wang, D., Gouhier, T.C., Menge, B.A., Ganguly, A.R., 2015. Intensification and spatial homogenization of coastal upwelling under climate change. *Nature* 518 (7539), 390–394.
- Weber, M.E., Wiedicke, M., Riech, V., Erlenkeuser, H., 1995. Carbonate preservation history in the Peru Basin: Paleooceanographic implications. *Paleoceanography* 10 (4), 775–800.
- Wells, P., Okada, H., 1996. Holocene and Pleistocene glacial palaeoceanography off southeastern Australia, based on foraminifers and nannofossils in Vema cored hole V18–222. *Aust. J. Earth Sci.* 43 (5), 509–523.